Supplemental figures and tables

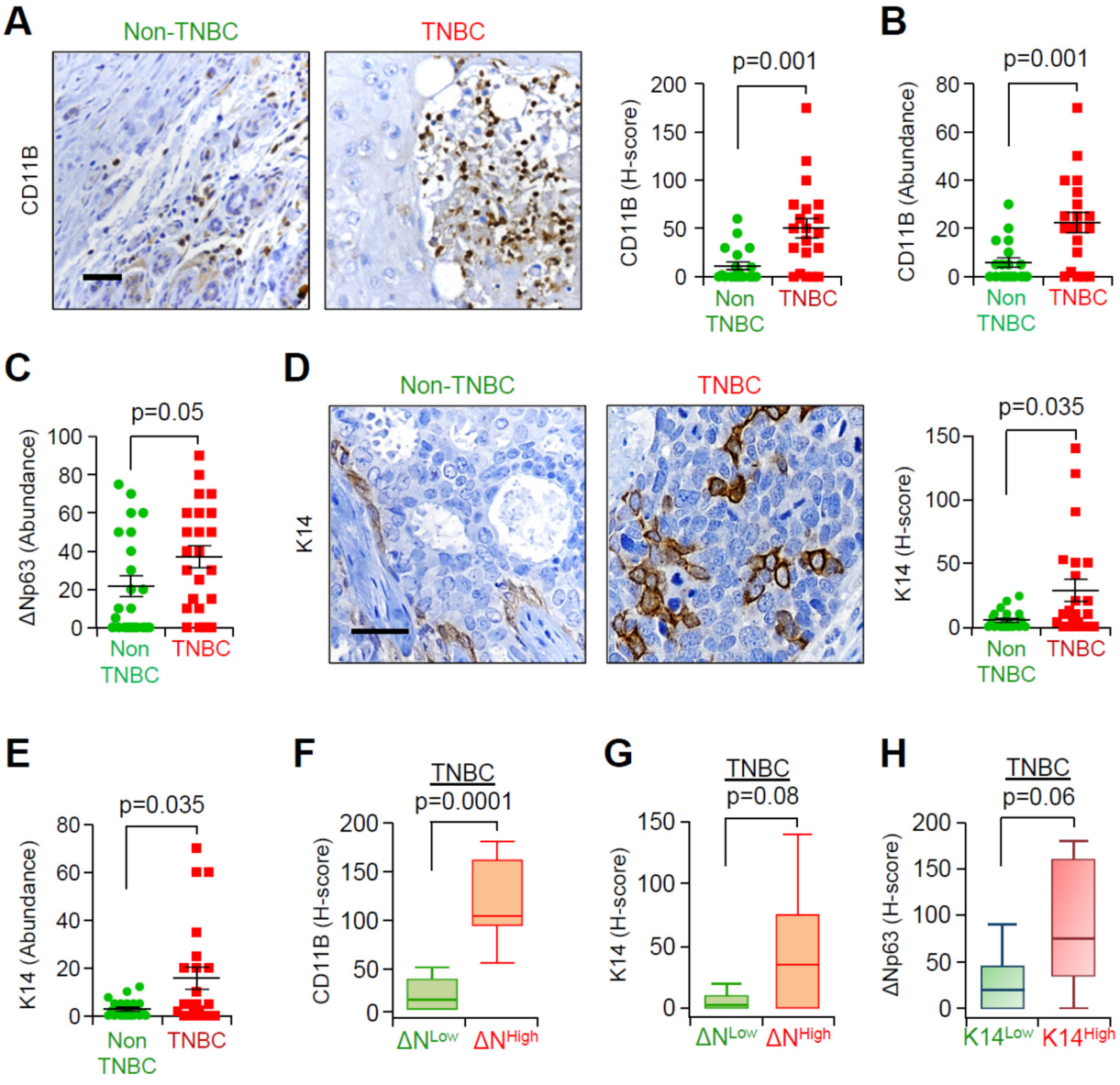

Supplemental Figure 1. Basal subset of TNBC represents higher CD11B⁺ cells infiltration in breast cancer. (**A-B**) Representative immunohistochemistry (IHC) images (**A**, left) and calculated H-score (**A**, right) and abundance (**B**) for CD11B⁺ cells in patient tissues. (**C**) Abundance of ΔNp63⁺ cells in patient tissues. (**D**) Representative IHC images (**D**, left) and

calculated H-score (**D**, right) and abundance (**E**) for K14 expression in patient tissues. (**A-E**) Non-TNBC n=21 patient samples, TNBC n=22 patient samples. The H-score value is the product of abundance of cells expressing respective protein (scale of 0-100) multiplied by the intensity of expression of that protein (scale of 0-3) (H-score= Abundance multiplied with Intensity). (**F**) Box plot is showing higher expression of CD11B in ΔNp63-high (ΔN^{high}) than ΔNp63-low (ΔN^{low}) human TNBC tissues. (**G**) Box plot is showing higher expression of K14 in ΔNp63-high (ΔN^{high}) than ΔNp63-low (ΔN^{low}) human TNBC tumor samples. ΔN^{high} and ΔN^{low} patients were stratified based on being above or below the median of ΔNp63 H-score in (main Figure, **1C**). (**H**) Box plot is showing ΔNp63 H-score in TNBC patient samples, which are stratified as $K14^{high}$ and $K14^{low}$ tissues by being above or below (respectively) median of K14 abundance. (**F-H**) n=22 TNBC patient samples. Scale bars, 40μm (**A-C**). (**A-C**) Mann-Whitney *U* test was used for scatter dot plots to calculate p-values.

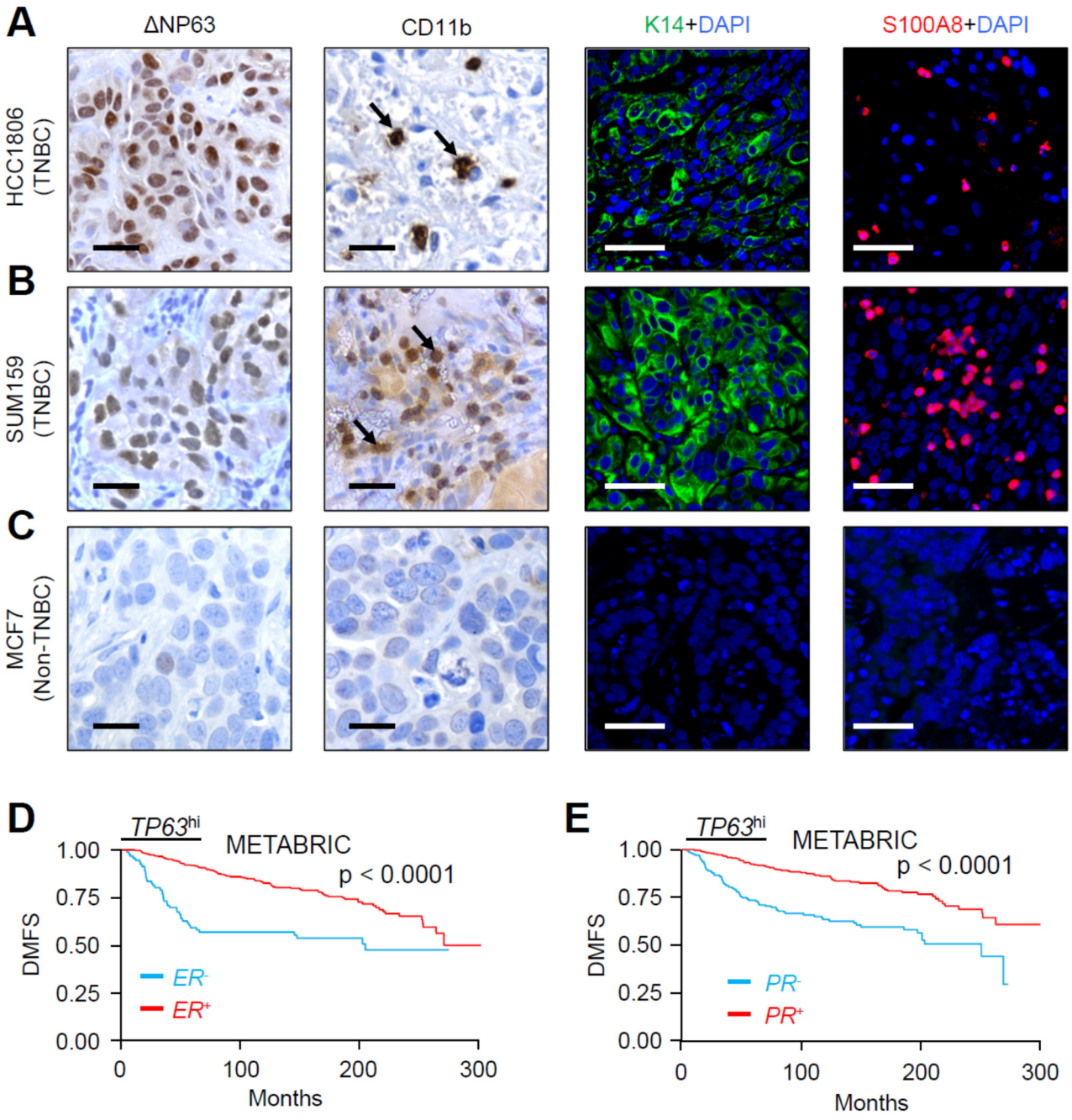

Supplemental Figure 2. TNBC cell line xenograft tumors have higher basal markers and CD11b^{+} cells infiltration.

(**A-C**) Representative IHC/IF images of TNBCs (HCC1806, SUM159) and non-TNBC (MCF7) xenograft tumors are showing increased ΔNp63^{+} cells, CD11B^{+} cells (black arrows), K14^{+} cells and S100A8^{+} cells in TNBCs compared to non-TNBCs (from left to right). (**D** and **E**)

Kaplan-Meier plot show that ER^- patients and PR^- patients have very poor prognosis ($p < 0.0001$) in p63-high patients (p63 expression was stratified into upper and lower quartile in patient samples). Published METABRIC dataset was used (1). Scale bars, 40μm (**A-C**). (**D** and **E**) Log-Rank test was used to compute *p*-values.

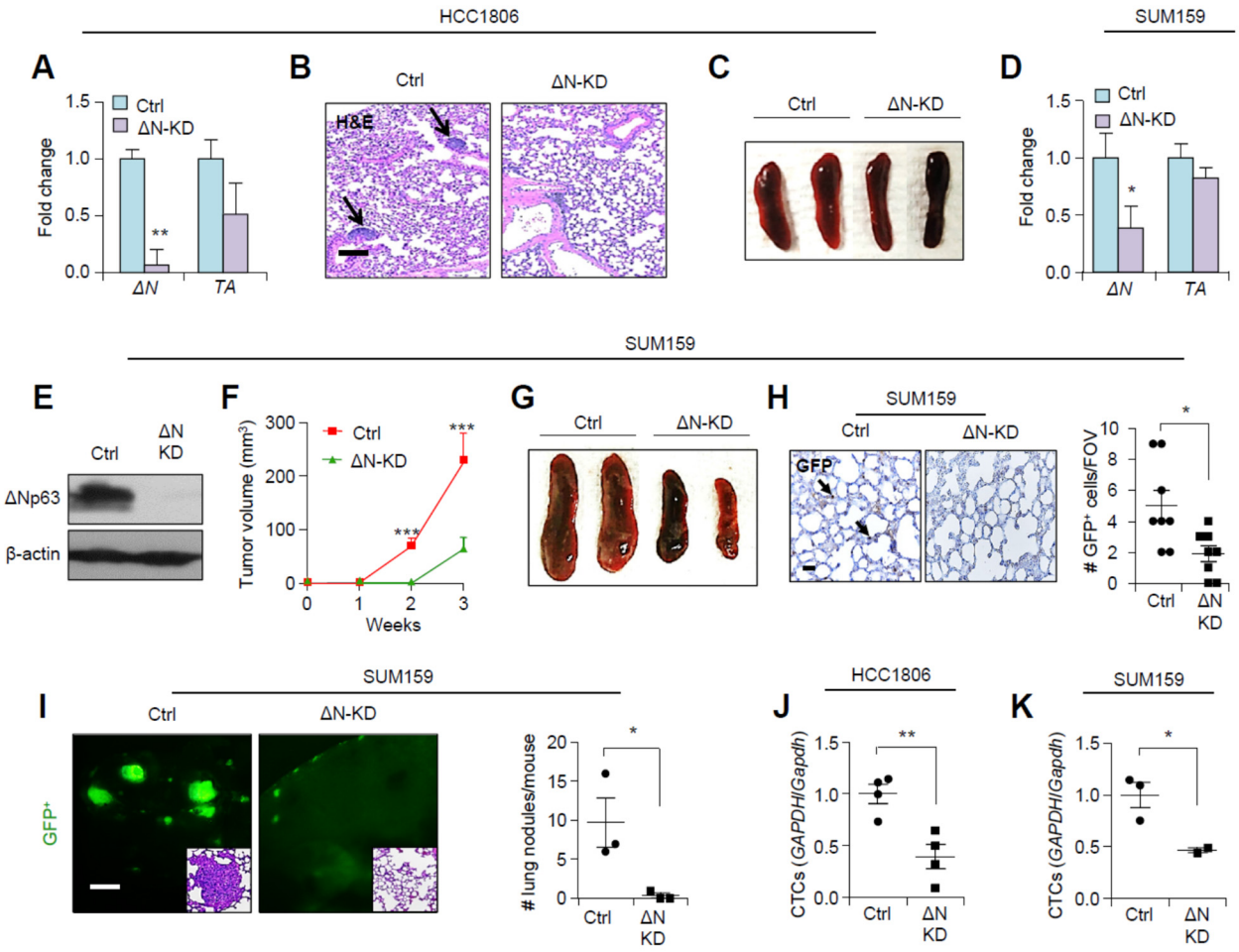

Supplemental Figure 3. ΔNp63 promotes tumor growth and metastasis in human TNBC. (**A**) qRT-PCR analysis of Δ*Np63* and *TAp63* mRNA expression in HCC1806 cells. (**B**) Representative H&E images are showing lung metastatic nodules (black arrows) in ΔNp63-KD HCC1806 xenograft tumor bearing mice compared to control. n=5 mice/group. (**C**) Representative spleen images of tumor bearing mice, n= 5 mice/group. (**D-E**) qRT-PCR and western blot analysis of Δ*Np63* and *TAp63* mRNA expression in SUM159 cells. (**F**) Tumor growth curve of GFP expressing control and ΔNp63-KD SUM159 cells. $5x10^5$ were injected/mammary gland. Ctrl n=7 mice and ΔN-KD n=6 mice. (**G**) Representative spleen images from tumor bearing mice, n=4 mice/group. (**H**) IHC image showing GFP^+ metastatic clusters and quantification in lungs of SUM159 xenograft tumor is shown in (right). n=4

mice/group. Multiple FOV/ lung was considered. (**I**) Fluorescence images are showing GFP^+ metastatic nodules (left) and quantification of metastasis in lungs of mice of resected SUM159 xenograft tumor in (right). Inset shows H&E images of sections of lung showing metastatic nodule in control only. n=3 mice/group. (**J-K**) Bar graph showing CTCs in mice injected with indicated group of HCC1806 cells (**J**) and SUM159 (**K**). CTC was calculated by semi-quantitative PCR of genomic DNA from peripheral blood using human *GAPDH* normalized with mouse *Gapdh*. All Real-time PCR values were normalized to the housekeeping gene *GAPDH*. Experiments were performed three times, each with qRT-PCR in technical duplicate, and data presented as the mean ± SD. Scale bars, 40μm (**B, H**), and 200μm (**I**). Data are presented as the mean ± SD in (**A**, **D**) and as the mean ± SEM in (**F**, **H-K**). *p<0.05, **p<0.01 and ***p<0.001. FOV; Field of view. (**F**) 2-way ANOVA test was performed with Bonferroni post-test adjustment. (**A, D, J, K**) Student's *t*-test was used .(**H**) Mann-Whitney *U* test was used.

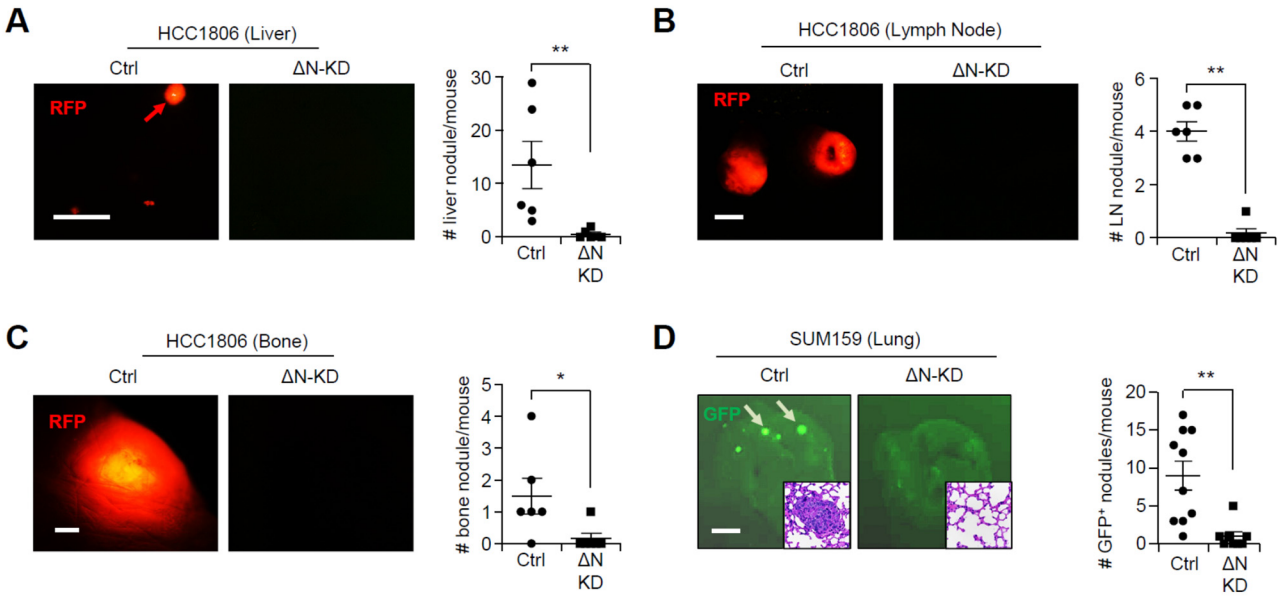

Supplemental Figure 4. ΔNp63 promotes metastasis in human TNBC. (**A**) Representative images of liver (**A**), lymph node (LN) (**B**), knee area of bone (**C**) are showing RFP$^+$ metastatic nodules of indicated groups. Bar graphs (**A-C**) represent the quantification of nodules in each metastatic site. Red arrow shows metastatic nodule in liver in **A**. (**D**) SUM159 cells ($2x10^5$) were injected into bloodstream of NSG mice via tail vein to study metastasis and representative image of GFP$^+$ nodules in lung of indicated groups (left), which is quantified in (right). White arrows show GFP$^+$ metastatic nodules in lung of mice injected with control cells only. Inset shows H&E image of lung metastatic nodule. n is indicated in scatter plots for different groups. (**A-C**) n=6 mice/group. Scale bar, 500μm (**A-D**). Data are presented as the mean ± SEM. *p<0.05 and **p<0.01. (**A-D**) Mann-Whitney *U* test was used to calculate *p*-values.

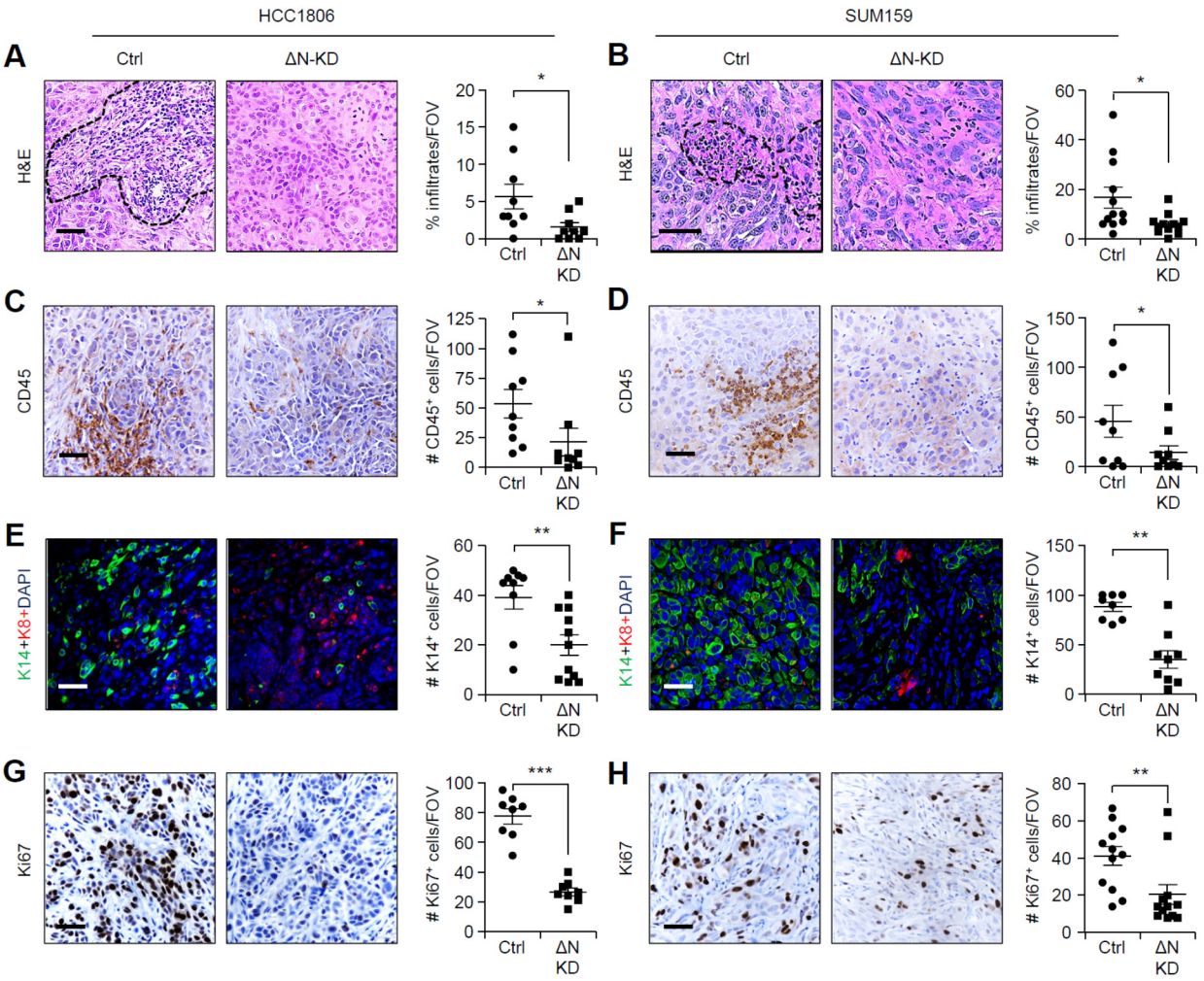

Supplemental Figure 5. Loss of ΔNp63 leads to dramatic alteration of tumor cell fate, reduced proliferation and immune infiltrate in TNBC. (**A** and **B**) Representative H&E images are showing immune cell infiltration in control and ΔNp63-KD HCC1806 (**A**) and SUM159 (**B**) primary tumors. (**C** and **D**) Representative IHC images are showing leukocytes marked by CD45 antibody in control and ΔNp63-KD HCC1806 (**C**) and SUM159 (**D**) primary tumors. (**E** and **F**) Representative IF images are showing the expression of luminal (K8) and basal (K14) markers are depicting cell fate change in ΔNp63-KD HCC1806 (**E**) and SUM159 (**F**) primary tumors compared to control. (**G** and **H**) Representative IHC images are showing the expression of cell proliferation (Ki67) in control and ΔNp63-KD HCC1806 (**G**) and

SUM159 (**H**) primary tumors. Bar graph on the right of each image represents respective quantification values. (**A-C, F-G**) Mann-Whitney *U* test and (**D, E, H**) Student's *t*-test was used to compute *p*-values. Scale bars, 40μm (**A-H**). *$p<0.05$, **$p<0.01$ and ***$p<0.001$. (**A-H**) n=6 samples were used and several random fields/sample were evaluated for quantification from 3 independent experiments. FOV; field of view. Bar graphs show data from 3 independent experiments and data presented as the mean ± SEM.

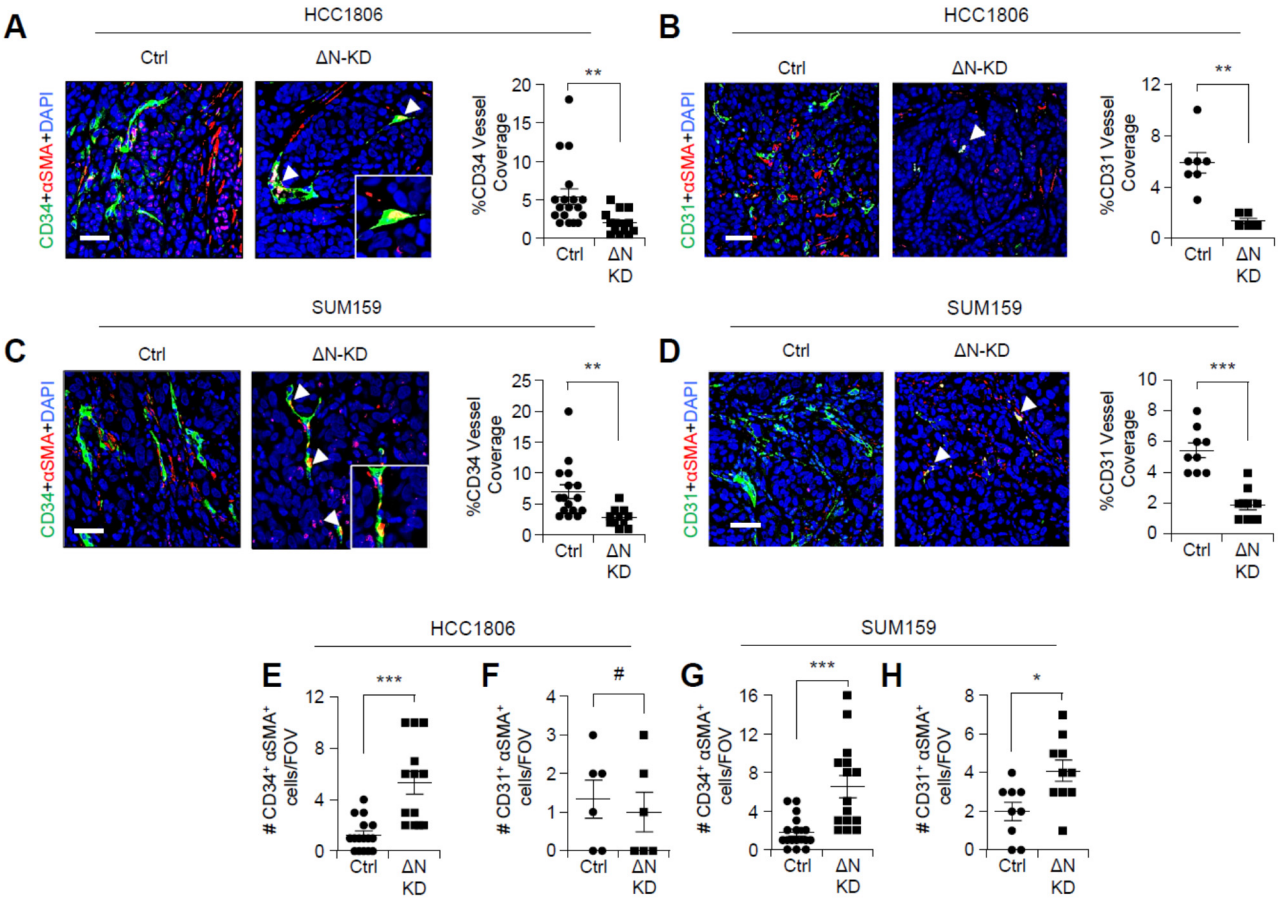

Supplemental Figure 6. Loss of ΔNp63 leads to reduce tumor angiogenesis in TNBC. (**A-D**) Representative IF images are showing angiogenesis markers such as CD34 and αSMA or CD31 and αSMA in control and ΔNp63-KD HCC1806 (**A** and **B**) and SUM159 (**C** and **D**) primary tumors. MVD (microvascular density) was evaluated in tumors of indicated groups. For MVD, $CD34^+$ or $CD31^+$ blood vessel coverage were evaluated (**A-D**, right). (**E-H**) Microvascular integrity (MVI) was measured in control and ΔNp63-KD HCC1806 and SUM159 tumors using combination of $CD34^+SMA^+$ or $CD31^+SMA^+$ markers. For MVI, $CD34^+SMA^+$ and $CD31^+SMA^+$ double-stained cells were evaluated. (**A-H**) Student's *t*-test was used to compute *p*-values. Scale bars, 40μm (**A-D**). **p*<0.05, ***p*<0.01, ****p*<0.001 and # = non-significant. n=4 samples were used and several random fields/sample were

evaluated for quantification from 3 independent experiments. Data presented as the mean ± SEM.

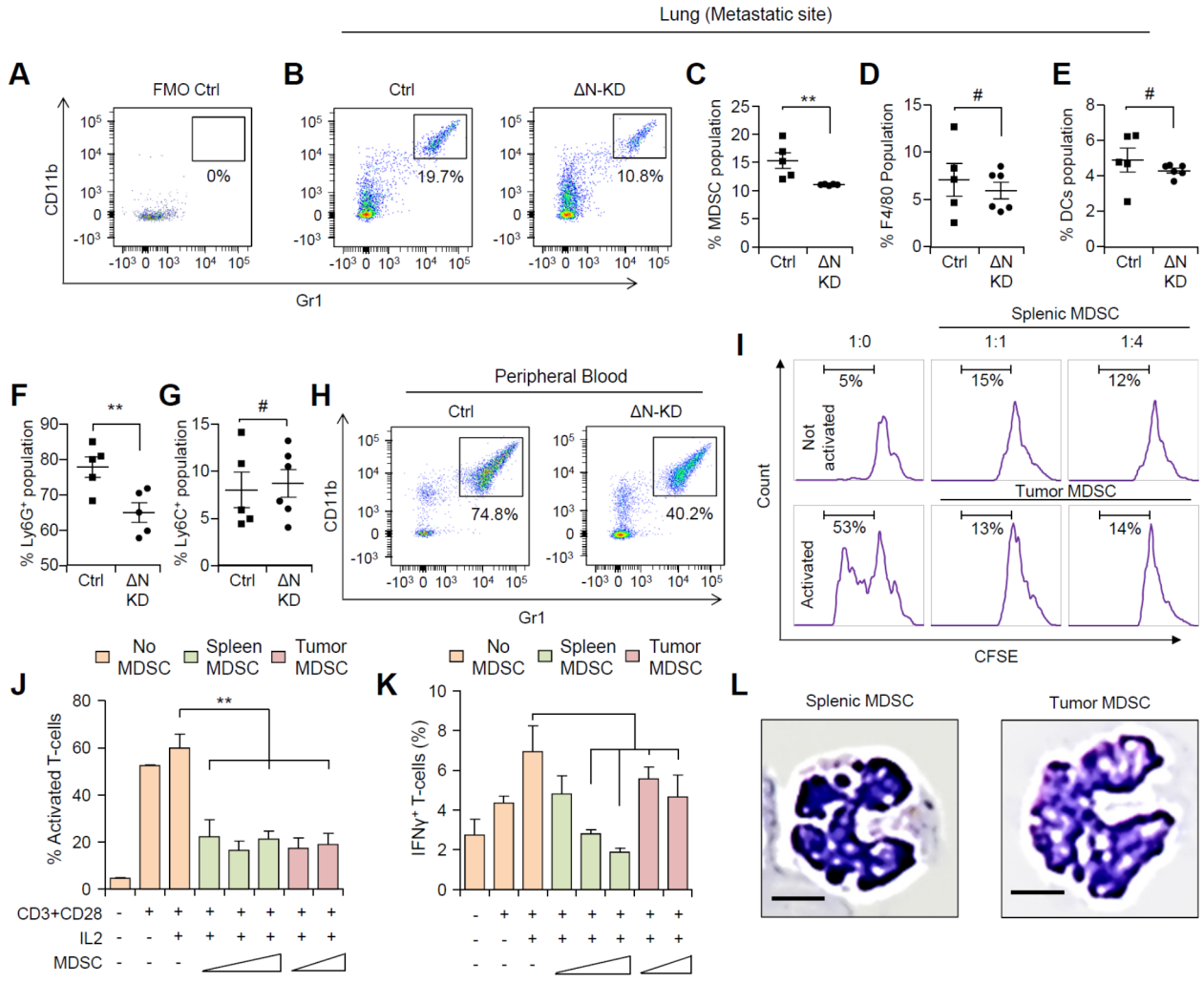

Supplemental Figure 7. ΔNp63 recruits tumor-induced PMN-MDSCs at metastatic site. (**A**) FMO control figure 3. FMO, Fluorescence Minus One control. (**B**) Flow profile of MDSCs in lungs of tumor bearing mice, based on the staining of CD45, CD11b and Gr1 markers. (**C-E**) Flow cytometric analysis of lungs of tumor bearing mice injected with control and ΔNp63-KD HCC1806 cells depicting $CD45^+$ tumor populations is showing percentage of (**C**) MDSCs ($CD11b^+$ $Gr1^+$ $F4/80^-$), (**D**) macrophages ($F4/80^+$), (**E**) DCs ($CD11c^+$). (**F, G**) Flow cytometric analysis is depicting MDSC sub-populations (**F**) PMN-MDSCs ($CD45^+CD11b^+Ly6G^+$ $Ly6C^{low}$) and (**G**) M-MDSCs ($CD45^+CD11b^+Ly6C^{high}$) in the lung of tumor bearing mice of

indicated groups. N is indicated in scatter plots of indicated groups for (**C-G**). (**H**) Flow profile of MDSC population of peripheral blood of mice injected with control and ΔNp63-KD HCC1806 cells. (**I, J**) CFSE-labeled splenocytes stimulated with anti-CD3, anti-CD28 monoclonal antibodies along with IL-2 treatment were co-cultured with MDSCs. MDSCs were either isolated from tumor or spleen of tumor bearing mice. Splenocytes were harvested from normal mice of same age (2). The cells were harvested and analyzed after 3-4 days using flow cytometry. CFSE dilution demonstrated that the proliferation of T-cells was inhibited by MDSCs (**I**), which is quantified (**J**). (**K**) The quantification of IFN-γ^+ splenocytes using flow cytometry analysis is showing inhibitory effects of MDSCs in a dose-dependent manner (1:2, 1:4 and 1:8 ratios were tested). (**I-K**) n=3 independent experiments performed in technical duplicate. Bar graphs show data presented as the mean ± SEM. (**L**) MDSCs after Giemsa staining. The MDSCs were isolated from primary mammary tumor or spleen of tumor-bearing mice. Scale bars, 5μm (**L**). Data are presented as the mean ± SEM. *p<0.05, **p<0.01 and #= non-significant. (**C-G**) Mann Whitney *U* test was used. (**J, K**) 1-way ANOVA with Tukey's post hoc test was used.

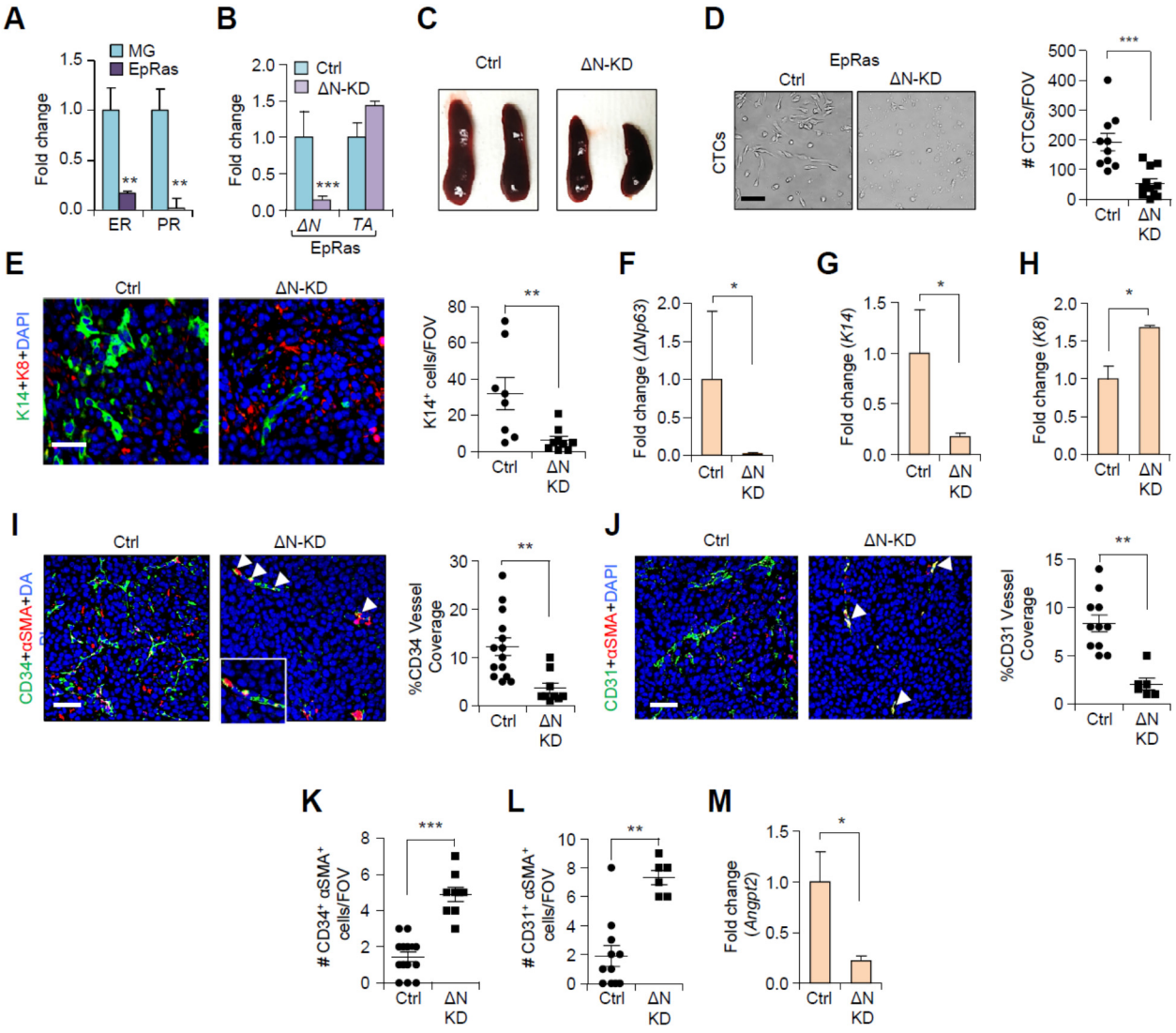

Supplemental Figure 8. Loss of ΔNp63 in mouse TNBC leads to reduced CTCs, cell fate and angiogenesis. (**A**, **B**) qRT-PCR analysis of Estrogen Receptor (*ER),* Progesterone Receptor *(PR)*, *ΔNp63* and *TAp63* mRNA expression in EpRas mouse TNBC cells. (**C**) Representative spleen images of tumor bearing mice of indicated groups, n=4 mice/group. (**D**) Images are showing circulating tumor cells (CTCs) from control and ΔNp63-KD EpRas xenograft bearing mice. Quantification is in right, n=4 mice/group. (**E**) Representative IF images are showing the expression of luminal (K8) and basal (K14) markers in tumors of indicated groups. Bar graph (right) represents quantification. (**F-H**) qRT-PCR data is showing

mRNA levels of ΔNp63 (**F**), cell fate markers K14 (**G**) and K8 (**H**) in control and ∆Np63-KD EpRas tumors. (**I-J**) Representative IF images showing angiogenesis markers such as CD34 and αSMA (**I**) or CD31 and αSMA (**J**) in control and ∆Np63-KD EpRas primary tumors. For MVD, $CD34^+$ or $CD31^+$ blood vessel coverage were evaluated of indicated groups (**I-J**, right). (**K-L**) For MVI, $CD34^+SMA^+$ and $CD31^+SMA^+$ double-stained cells were evaluated. White arrowheads show double positive $CD31^+$ SMA^+ (yellow) cells in ∆Np63-KD tumors. n=4 samples were used and several random fields/sample were evaluated. Bar graphs show data from 3 independent experiments. (**M**) qRT-PCR data is showing mRNA levels of Angiopoietin2 (Angpt2) in indicated tumors. (**A, B, F-H** and **M**) All Real-time PCR values were normalized to the housekeeping gene *Gapdh*. Experiments were performed three times, each with qRT-PCR in technical duplicate, and data presented as the mean ± SD. (**F-H, M**) n=4 tumors/group. Bar graph on the right of each image represents the quantifications. (**A, B, D, E, H-L**) Student's *t*-test and (**F-G, M**) Mann-Whitney *U* test was used. Scale bar, 40μm (**D, E, I** and **J**). Data are presented as the mean ± SEM. *p<0.05, **p<0.01 and ***p<0.001.

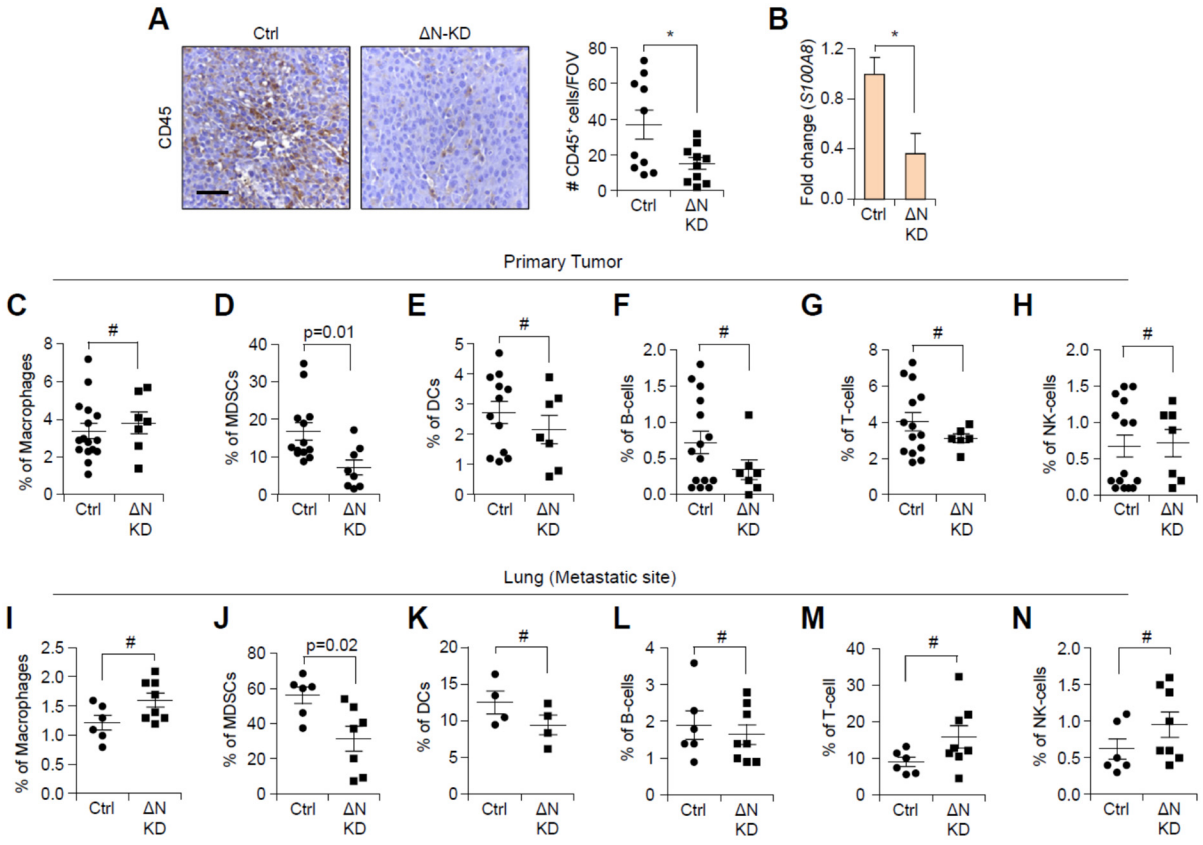

Supplemental Figure 9. Loss of ΔNp63 in mouse TNBC leads to reduced PMN-MDSC infiltration in primary tumor and metastatic lungs. (**A**) Representative IHC images of primary tumors are showing leukocytes infiltration marked by CD45 antibody from control and ΔNp63-KD EpRas tumors. Quantification is shown in the right panel. n=3 samples were used and several random fields/sample were evaluated for quantification. Bar graphs show data from 3 independent experiments and data presented as the mean ± SEM. (**B**) qRT-PCR analysis is showing mRNA levels of S100A8 in control and ΔNp63-KD EpRas tumors are showing reduced S100A8 mRNA in ΔNp63-KD tumors compared to control. n=4 samples/group. Real-time PCR values were normalized to the housekeeping gene *Gapdh*. Experiments were performed three times, each with qRT-PCR in technical duplicate, and data presented as the mean ± SD. (**C-H**) Flow cytometric analysis is depicting percentage

of (**C**) Macrophages ($CD45^+F4/80^+$), (**D**) MDSCs ($CD45^+CD11b^+Gr1^+F4/80^-$), (**E**) dendritic cells (DCs; $CD45^+CD11c^+$), (**F**) B-cells ($CD45^+CD19^+$), (**G**) T-cells ($CD45^+CD3^+$) and (**H**) NK-cells ($CD45^+CD49b^+$) in EpRas-derived primary tumors grown in BALB/c mice. (**I-N**) Flow cytometric analysis is depicting percentage of (**I**) Macrophages ($CD45^+F4/80^+$), (**J**) MDSCs ($CD45^+CD11b^+Gr1^+F4/80^-$), (**K**) dendritic cells (DCs; $CD45^+CD11c^+$), (**L**) B-cells ($CD45^+CD19^+$), (**M**) T-cells ($CD45^+CD3^+$) and (**N**) NK-cells ($CD45^+CD49b^+$) in the lungs of EpRas tumor bearing BALB/c mice. n is indicated in scatter plots for different groups (**C-N**). (**A-N**) Mann-Whitney *U* test was used to compute *p*-value. Scale bar, 40μm (**A**). Data are presented as the mean ± SEM. *$p<0.05$ and #= non-significant. FOV; field of view.

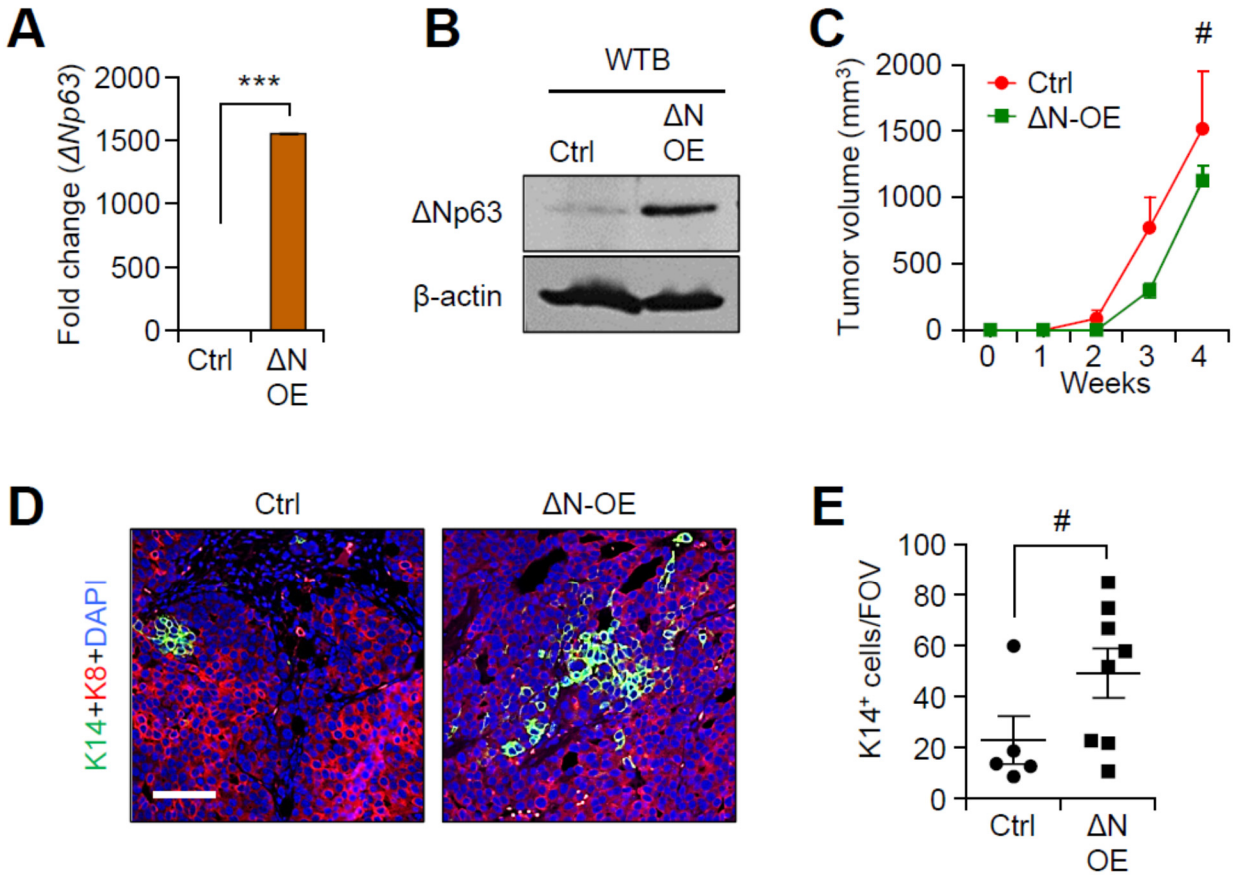

Supplemental Figure 10. Overexpression of ΔNp63 alters cell fate but not tumor growth in non-TNBC tumors. (**A**) qRT-PCR and (**B**) western blot are showing ΔNp63 (ΔN) mRNA and protein levels in WTB luminal cells (non-TNBC) after lentivirus-mediated overexpression (OE) of ΔNp63. Real-time PCR values were normalized to the housekeeping gene *Gapdh*. Experiments were performed three times, each with qRT-PCR in technical duplicate, and data presented as the mean ± SD. (**C**) Tumor growth curves in mice injected with control and ΔNp63-OE WTB cells. Briefly, ($2x10^5$) were injected into mammary fat pad (MFP) of FVB mice and tumor were palpated for indicated time periods. n=6 tumors/group. (**D, E**) Representative IF images are showing increased expression of basal (K14) marker are depicting cell fate change in ΔNp63-OE WTB primary tumors compared to control. n=3 samples were used and several random fields/sample were evaluated for quantification. Bar

graph (**E**) represents quantification and data is presented as the mean ± SEM. (**A, E**) Mann-Whitney *U* test was used to compute p-values. (**C**) 2-way ANOVA was performed with a Bonferroni post-correction to compute statistical significance of tumor growth. Scale bar, 80μm (**D**). Data are presented as the mean ± SD for (**A**) and data are presented as the mean ± SEM for (**C, E**). ***p<0.001 and # = non-significant. FOV; field of view.

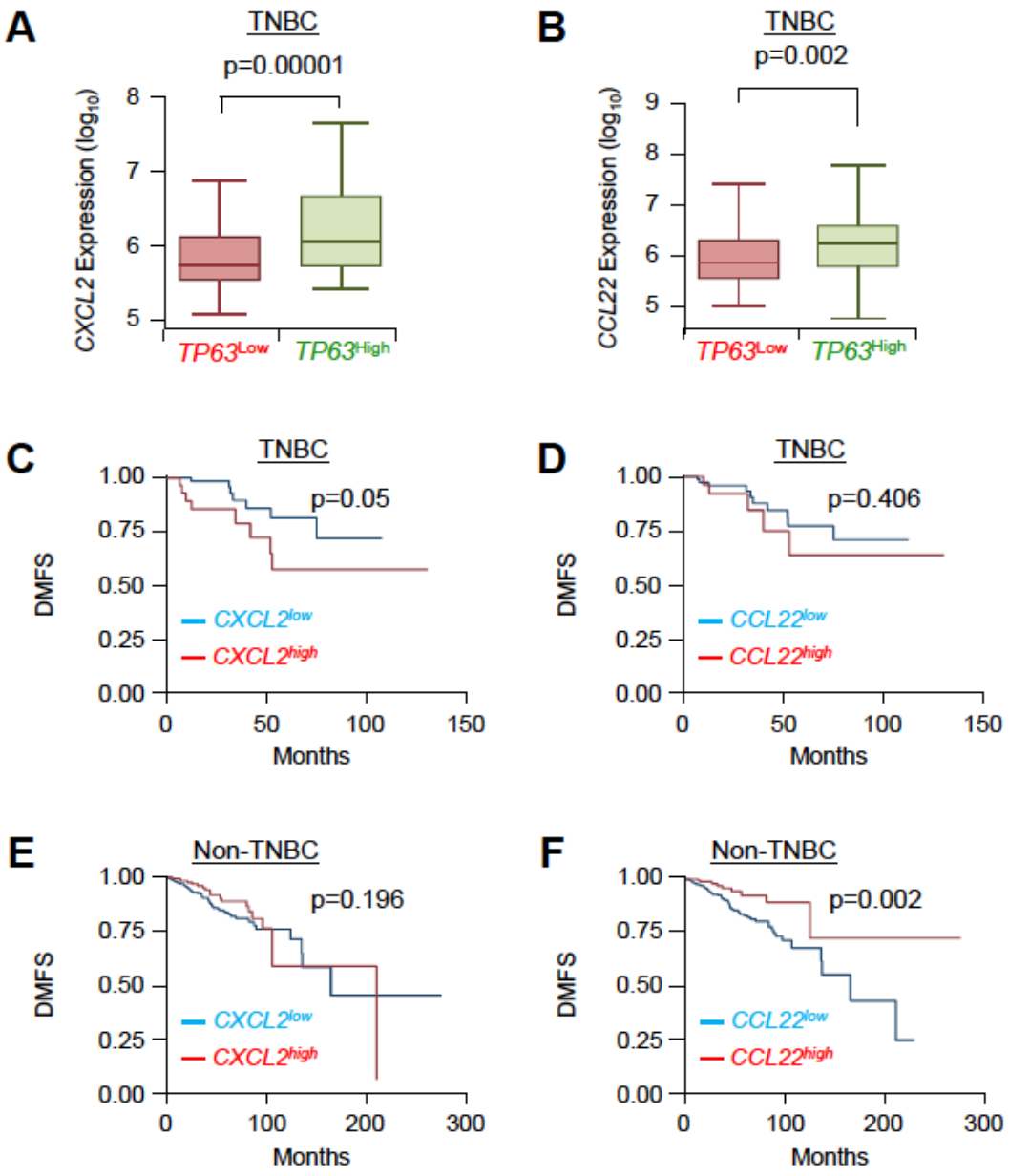

Supplemental Figure 11. TNBC patient tumors express higher *CXCL2* and *CCL2* and this high expression of *CXCL2* and *CCL22* is associated with poor distant metastasis-free survival of patients. (**A, B**) Box plots are showing positive correlation between *TP63* and *CXCL2* (**A**) and *CCL22* (**B**) respectively in ER$^-$PR$^-$HER2$^-$TNBC subsets. (**C, D**) High *CXCL2* and *CCL22* correlate with poor distant metastasis-free survival (DMFS) in TNBC

patients. (**E-F**) On the contrary, high *CXCL2* and *CCL22* correlates with better DMFS in non-TNBC patients. TCGA dataset was used for clinical dataset analysis (3). (**A, B**) Mann-Whitney *U* test was used to compute *p*-value. (**C-F**) Log-Rank test was used for KM plots to calculate *p*-values.

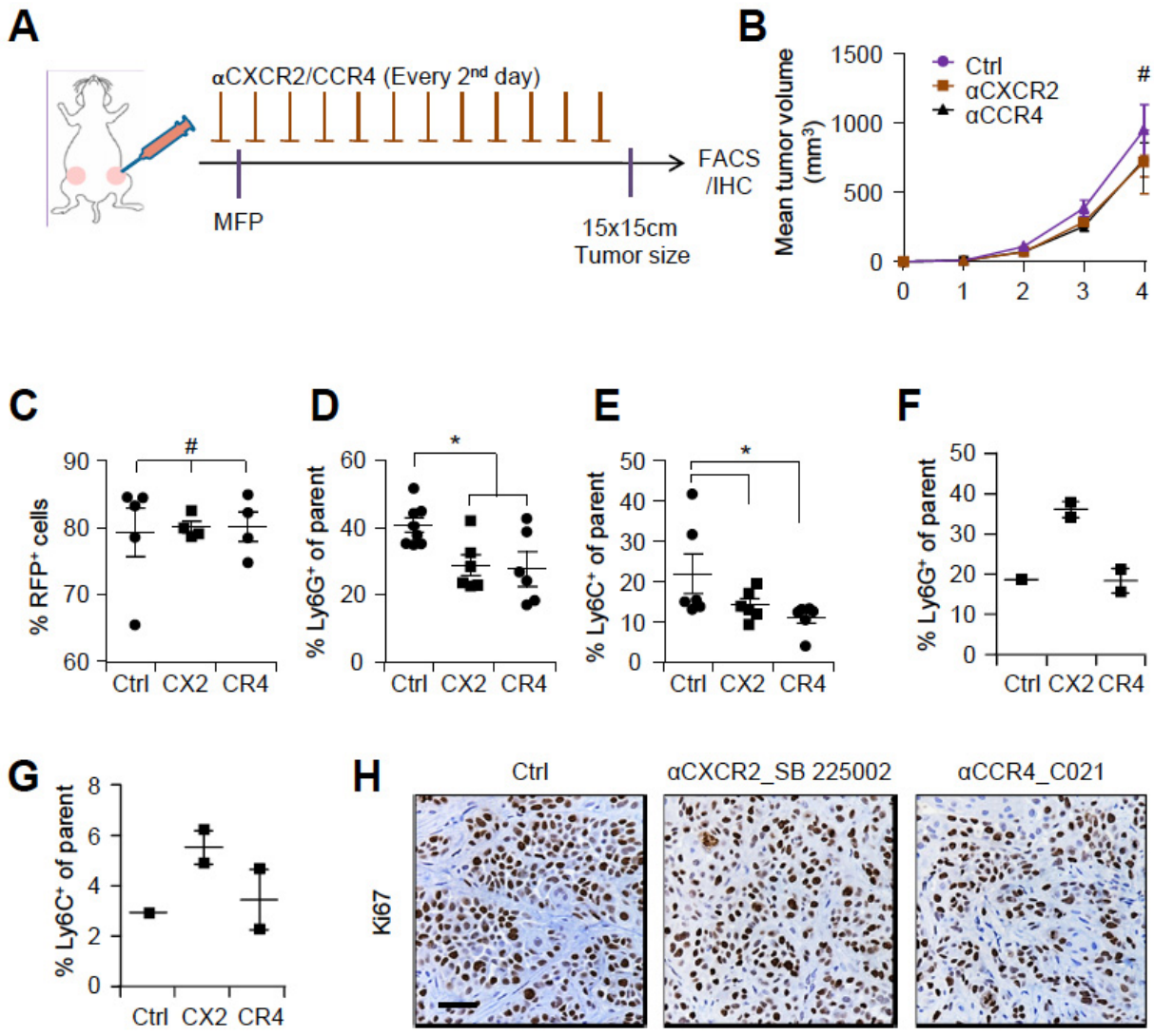

Supplemental Figure 12. Blockade of MDSC recruitment does not alter primary tumor growth. (**A**) Schematic describing the experimental strategy for blocking chemokine receptors in spontaneous metastasis model. Mice were pre-treated with chemokine blockers 2 days before injection of tumor cells and treatment continued every 2nd day. (**B**) HCC1806 tumor cells ($2x10^5$) were injected into mammary fat pad of Nude mice are showing tumor growth curve upon blocking of indicated chemokine receptors. Ctrl n=8 mice tumors, CXCR2 inhibitor n=4 mice tumors and CCR4 inhibitor n=4 mice tumors. (**C-E**) Flow cytometry analysis representing the percentage of PMN-MDSCs ($Ly6G^+$) (**C**) M-MDSCs ($Ly6C^+$) (**D**) and RFP^+

tumor cells (**E**) in the primary tumor of HCC1806 cells upon indicated treatments. (**F** and **G**) Flow cytometric analysis is depicting $Ly6G^+$ and $Ly6C^+$ MDSCs in blood of tumor bearing mice of indicated groups. N is indicated in scatter plots for different groups. (**H**) IHC analysis of treated and untreated primary mammary tumors is showing no difference in $Ki67^+$ cells between indicated groups. n=3 samples were used and several random fields/sample were evaluated for quantification from 3 independent experiments. Scale bars, 40μm (**H**). Data are presented as the mean ± SEM. *p<0.05 and # = non-significant. (**B**) 2-way ANOVA with Bonferroni post-test was used to compute statistical significance for tumor growth curve data. (**C-E**) 1-way ANOVA was used with Tukey's post hoc test to compute p-values.

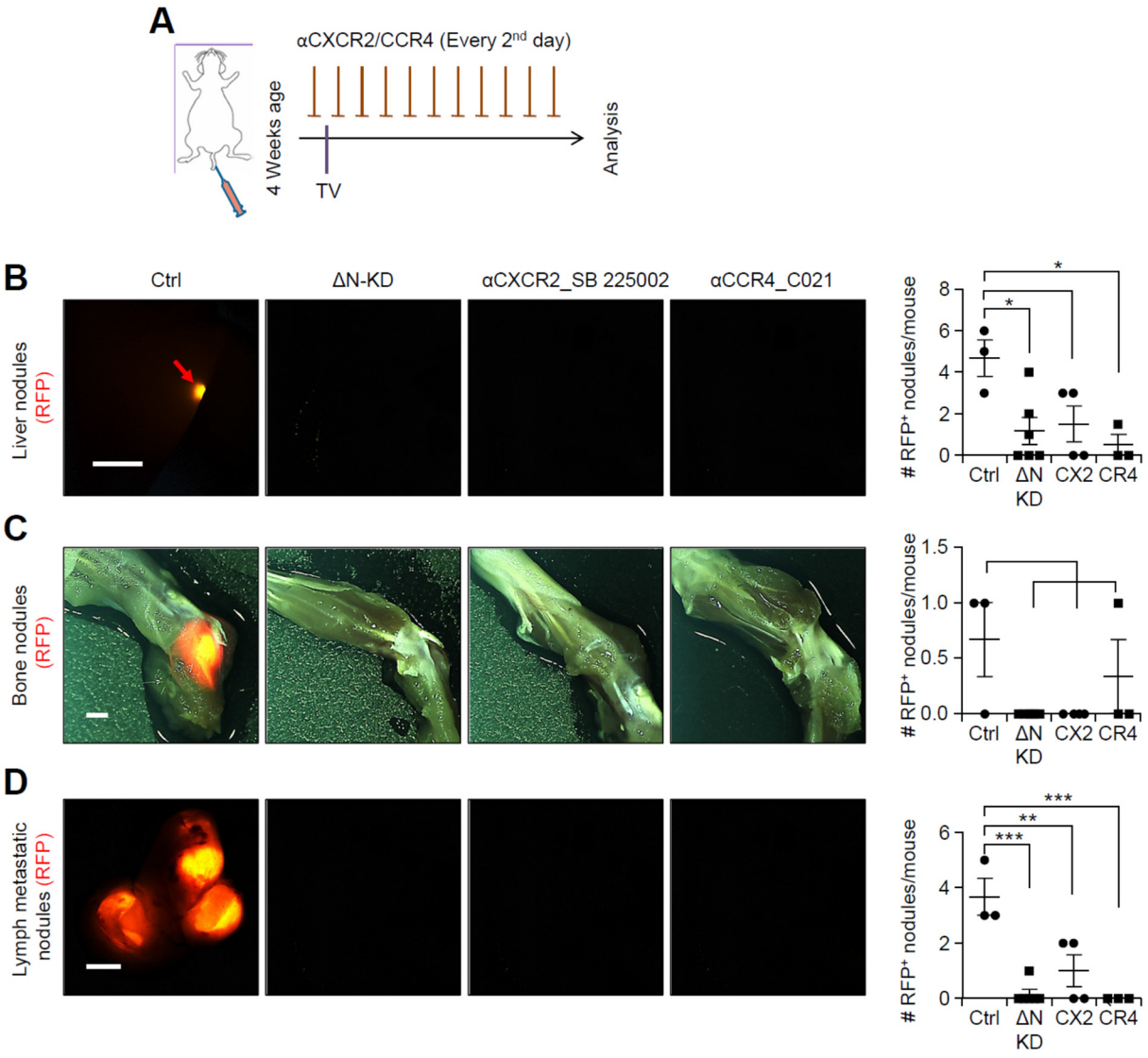

Supplemental Figure 13. Blockade of MDSC recruitment significantly diminishes metastasis. (**A**) Schematic describing the experimental strategy for blocking chemokine receptors in experimental metastasis model. Mice were pre-treated with chemokine blockers 2 days before injection of tumor cells and treatment continued every 2nd day. (**B-D**) RFP images of HCC1806 tumor cells in distal metastatic sites after cells were injected via tail vein to NSG mice. Mice were started on treatment with the CXCR2 or CCR4 inhibitors following schematic diagram in (**A**). Representative images are showing RFP+ metastatic nodules (red arrow) in the liver (**B**), knee joint at bone (**C**) and lymph nodes (**D**). Scatter plots are showing

quantification of RFP^+ nodules in the respective organs (**B-D**). Ctrl n=4 mice, ΔN-KD n=6 mice, αCXCR2 n=4 mice and αCCR4 n=3 mice in (**B-D**). Scale bars, 200μm (**B**), 500μm (**C** and **D**). Data are presented as the mean ± SEM. 2 independent experiments were performed. **p*<0.05, ***p*<0.01 and ****p*<0.001. (**B-D**) 1-way ANOVA was used with Tukey's post hoc test to compute *p*-values.

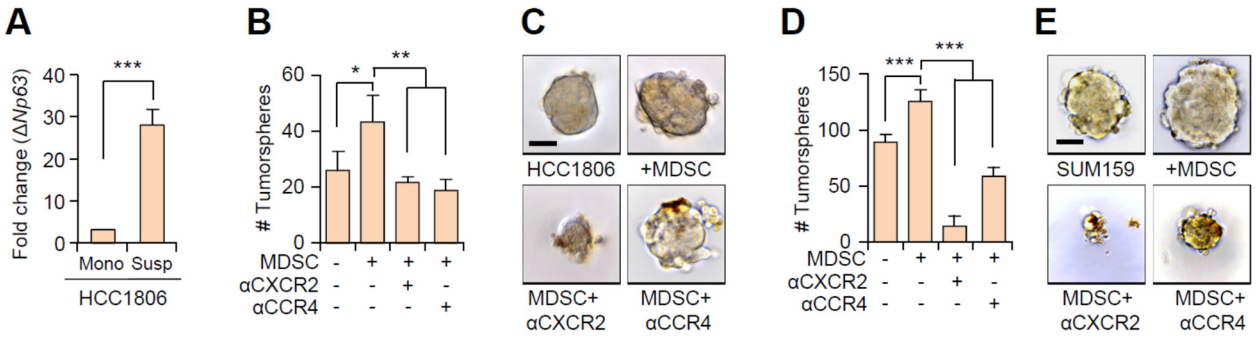

Supplemental Figure 14. ΔNp63 is enriched in CSCs and reduced level of MDSCs decreases CSC function. (**A**) qRT-PCR analysis of the expression of ΔNp63 in HCC1806 cells cultured in monolayer *vs*. in suspension. In suspension cultures enrich for stem cell activity in tumorspheres. Real-time PCR values were normalized to the housekeeping gene *GAPDH*. Experiments were performed three times, each with qRT-PCR in technical duplicate, and data presented as the mean ± SD. Bar graphs are showing tumorspheres number (**B**) and representative images (**C**) of HCC1806 cells cultured for 3 days with indicated treatments. n=3 independent experiments performed in technical duplicate. (**D** and **E**) Bar graphs are showing tumorspheres number (**D**) and representative images (**E**) of SUM159 cells cultured for 3 days with indicated treatments (**E**) n=3 independent experiments performed in technical duplicate. Scale bars, 40μm (**C** and **E**). Data are presented as the mean ± SEM. **p*<0.05, ***p*<0.01 and ****p*<0.001. (**A**) Student's *t*-test was used to compute *p*-value. (**B, D**) 1-way ANOVA was used with Tukey's post hoc test to compute *p*-values.

Fig. 2A

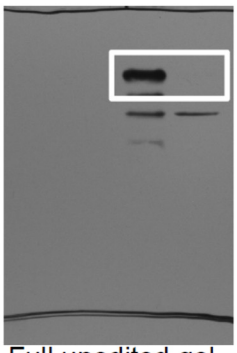

Full unedited gel for Figure 2A (Top lane)

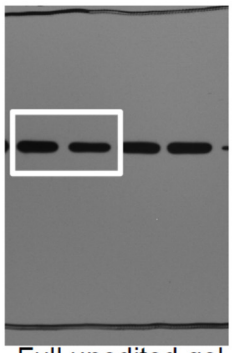

Full unedited gel for Figure 2A (Bottom lane)

Supplemental Fig. 3E

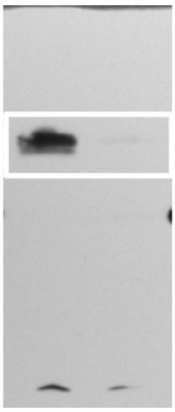

Full unedited gel for Supplemental Figure 3E (Top lane)

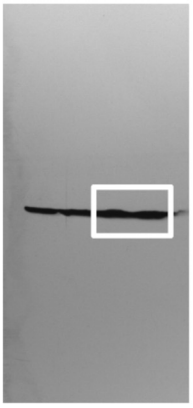

Full unedited gel for Supplemental Figure 3E (Bottom lane)

Fig. 4A

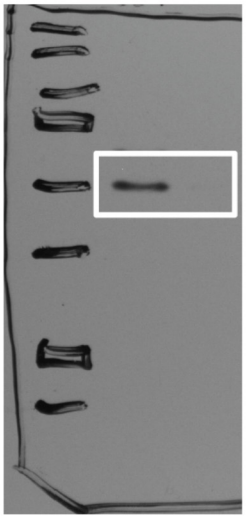

Full unedited gel for Figure 4A (Top lane)

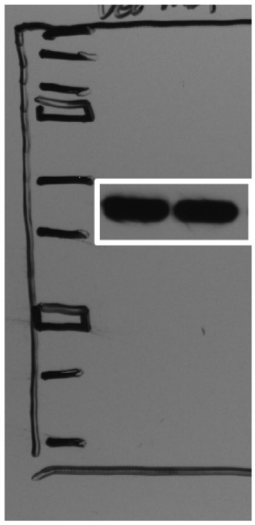

Full unedited gel for Figure 4A (Bottom lane)

Supplemental Fig. 10B

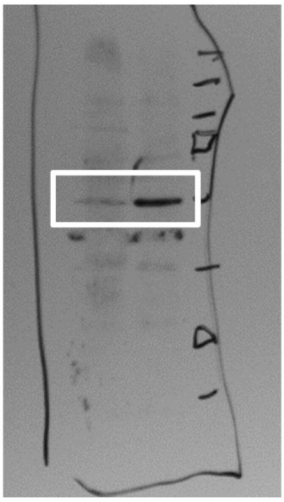

Full unedited gel for Supplemental Figure 10B (Top lane)

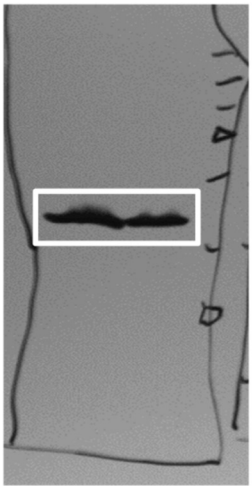

Full unedited gel for Supplemental Figure 10B (Bottom lane)

Supplemental Figure 15. Uncut gels of all western blot images.

Supplemental Table 1: Antibody used for IHC, IF and Western blot

Antibody	***Catalog number***	***Dilution (application)***	***Company***
GFP	ab13970	1:500 (IHC)	Abcam
ΔNp63	RR14 clone	1:75 (IHC), 1:1000 (Western Blot)	Romano et al, 2012
β-actin	ab6276	1:10,000 (Western Blot)	Abcam
K8	TROMA-1s	1:25 (IF)	DSHB
K14	PRB155P	1:200 (IF)	Biolegend
Ki67	Ki67-MM1-L-CE	1:50 (IHC)	Leica Microsystems
Cleaved-caspase-3	9661S	1:100 (IHC)	Cell Signaling
CD31	ab28364	1:100 (IHC)	Abcam
CD34	ab81289	1:200 (IF)	Abcam
αSMA	ab7817	1:200 (IF)	Abcam
S100A8	MAB3059-SP	1:200 (IF)	R&D Systems
S100A9	ab92507	1:250 (IF)	Abcam
CD33	NCL-L-CD33	1:10 (IF)	Leica Microsystems
CD11B	ab133357	1:1000 (IHC)	Abcam
CD45	550539	1:12.5 (IHC)	BD Biosciences
CD15	555400	1:200 (IF)	BD Biosciences
LOX-1	Ab126538	1:200 (IF)	Abcam

Supplemental Table 2: Antibody used for flow cytometry

Antibody	***Fluorochrome***	***Dilution***	***Catalog number***	***Company***
CD11c	APC	1:100	#550261	BD Biosciences
F4/80	APC-Cy7	1:100	#123118	Biolegend
CD45	PE-Cy7	1:100	#552848	BD Biosciences
CD11b	Per-CP-Cy5.5	1:100	#550993	BD Biosciences
Ly-6C	APC	1:100	#560595	BD Biosciences
Ly-6G	FITC	1:100	#551460	BD Biosciences
CD45	FITC	1:100	#553080	BD Biosciences
Gr1	APC-Cy7	1:100	#557661	BD Biosciences
F4/80	FITC	1:100	#11-4801-81	Invitrogen
Ly6G	V450	1:100	#560603	BD Biosciences
CD49b	PE	1:100	#553858	BD Biosciences
CD3e	PerCP-Cy5.5	1:100	#551163	BD Biosciences
CD19	APC	1:100	#550992	BD Biosciences

Supplemental Table 3: Primers (human and mouse genes) used in quantitative PCR

GENE	*FORWARD*	*REVERSE*
hΔNP63	GGAAAACAATGCCCAGACTC	GTG GAA TAC GTC CAG GTG GC
hTAP63	AAGATG GTG CGA CAA ACA AG	AGA GAG CAT CGA AGG TGG AG
hGAPDH	GGAGTCAACGGATTTGGTCGTA	GGCAACAATATCCACTTTACCAGAGT
hCXCR2	TGG ATT TTT GGC ACA TTC C	TGG GCT AAC ATT GGA TGA GT
hCCR4	AGA AGG CAT CAA GGC ATT TGG	ACA CAT CAG TCA TGG ACC TGA G
hCXCL1	AGT CAT AGC CAC ACT CAA GAA TGG	GAT GCA GGA TTG AGG CAA GC
hCXCL2	CGC CCA AAC CGA AGT CAT AG	AGA CAA GCT TTC TGC CCA TTC T
hCXCL3	TCC CCC ATG GTT CAG AAA ATC	GGT GCT CCC CTT GTT CAG TAT CT
hCXCL6	AGA GCT GCG TTG CAC TTG TT	GCA GTT TAC CAA TCG TTT TGG GG
hCXCL8	AGC TGG CCG TGG CTC TCT	CTG ACA TCT AAG TTC TTT AGC ACT CCT T
hCXCL10	GTG GCA TTC AAG GAG TAC CTC	GCC TTC GAT TCT GGA TTC AGA CA
hCXCL11	TTG GCT GTG ATA TTG TGT GCT	GGA TTT AGG CAT CGT TGT CCT TT
hCXCL17	TCC ATG GTC TCT AGC AGC CT	GGG GCT CTC AGG AAC CAA TC
hCCL2	CAG CCA GAT GCA ATC AAT GCC	TGG AAT CCT GAA CCC ACT TCT
hCCL5	CCA GCA GTC GTC TTT GTC AC	CTC TGG GTT GGC ACA CAC TT
hCCL17	AGG GAG CCA TTC CCC TTA GA	TGT TGG GGT CCG AAC AGA TG
hCCL22	ATC GCC TAC AGA CTG CAC TC	GAC GGT AAC GGA CGT AAT CAC

GENE	*FORWARD*	*REVERSE*
mΔNp63	TGC CCA GAC TCA ATT TAG TGA	GAG GAG CCG TCC TGA ATC TG
mTAp63	CTC GTG GAA AGA AAG TTA TTA C	GGG CTG TAC TGA GCA TAT AG
mGapdh	TTC CAC TCT TCC ACC TTC GAT GC	GGG TCT GGG ATG GAA ATT GTG AGG

mCxcr2	ATG CCC TCT ATT CTG CCA GAT	GTG CTC CGG TTG TAT AAG ATG AC
mCcr4	GGA AGG TAT CAA GGC ATT TGG G	GTA CAC GTC CGT CAT GGA CTT
Cxcl1	TGA GCT GCG CTG TCA GTG CCT	AGA AGC CAG CGT TCA CCA GA
Cxcl2	GAG CTT GAG TGT GAC GCC CCC AGG	GTT AGC CTT GCC TTT GTT CAG TAT C
mER	AAT GCA AGA ACG TTG TGC CC	TCT GCT TCC GGG GGT ATG TA
mPR	GTG TCG TCT GTA GTC TCG CC	GAG AAA GCT CCC TCC ACG TC
mCxcl3	CCA TCC AGA GCT TGA CGG TG	TGG GGG TTG AGG CAA ACT TC
mCxcl10	CCA AGT GCT GCC GTC ATT TTC	TCC CTA TGG CCC TCA TTC TCA
mCcl2	TTA AAA ACC TGG ATC GGA ACC AA	GCA TTA GCT TCA GAT TTA CGG GT
mCcl3	TGT ACC ATG ACA CTC TGC AAC	CAA CGA TGA ATT GGC GTG GAA
mCcl5	GCT GCT TTG CCT ACC TCT CC	TCG AGT GAC AAA CAC GAC TGC
mCcl17	TAC CAT GAG GTC ACT TCA GAT GC	GCA CTC TCG GCC TAC ATT GG
mCcl22	AGG TCC CTA TGG TGC CAA TGT	CGG CAG GAT TTT GAG GTC CA
mKeratin14	AGG GCT CTT GTG GTA TCG GT	ACC ATA GCC ACC TCC AAT CC
mKeratin8	AGG ACT GAC CGA CGA GAT CA	CTC GTA CTG GGC ACG AAC TT
mAngiopoietin2	CCA ACT CCA AGA GCT CGG TT	CGG TGT TGG ATG ACT GTC CA
mS100A8	AGA AGG CCT TGA GCA ACC TC	ATC GCA AGG AAC TCC TCG AA

GENE	*FORWARD*	*REVERSE*
Human GAPDH (Genomic)	CTG GGC TAC ACT GAG CAC C	AAG TGG TCG TTG AGG GCA ATG
Mouse Gapdh (Genomic)	AAC ATC AAA TGG GGT GAG G	GGC CTT CTC CAT GGT GGT

Supplemental Table 4: Recombinant proteins and synthetic antagonists

Protein/compound	*Company*	*Catalog number*	*Activity*
Recombinant Human CXCL2	R&D Systems	276-GB	
Recombinant Human CCL22	R&D Systems	336-MD	
SB255002	Tocris Bioscience	2725	Cxcr2 blocker
C021 Dihydrochloride	Tocris Bioscience	3581	Ccr4 Blocker
Recombinant Mouse Chitinase 3-like 1 Protein	R&D Systems	2649-CH-050	
Recombinant Mouse MMP-9 Protein	R&D Systems	909-MM-010	

1. Curtis C, Shah SP, Chin SF, Turashvili G, Rueda OM, Dunning MJ, Speed D, Lynch AG, Samarajiwa S, Yuan Y, et al. The genomic and transcriptomic architecture of 2,000 breast tumours reveals novel subgroups. *Nature.* 2012;486(7403):346-52.
2. Welte T, Kim IS, Tian L, Gao X, Wang H, Li J, Holdman XB, Herschkowitz JI, Pond A, Xie G, et al. Oncogenic mTOR signalling recruits myeloid-derived suppressor cells to promote tumour initiation. *Nat Cell Biol.* 2016;18(6):632-44.
3. Cancer Genome Atlas N. Comprehensive molecular portraits of human breast tumours. *Nature.* 2012;490(7418):61-70.